University of Sistan and Baluchestan

Challenges in Nano and Micro Scale Science and Technology

Online ISSN: 2821 - 000X

Green-Synthesized Graphene Based TiO_2 Nanocomposite with High Photocatalytic Efficiency for Water Purification

Arash Khoshnoodfar[1]✉ | Sanaz Khammar[2] | Ehsan Moeini Feyzabadi[3]

1 Department of Environmental Engineering, Faculty of Natural Resources and Environment, University of Birjand, Birjand, Iran. Email: Arash.khoshnoodfar@birjand.ac.ir

2 Department of Landscape Design Engineering, Faculty of Geography and Environmental Planning, University of Sistan & Baluchestan, Zahedan, Iran.

3 Department of Environmental Engineering, Faculty of Natural Resources and Environment, University of Birjand, Birjand, Iran.

Article Info

Article type:
Research Article

Keywords:
Graphene,
Photocatalysis,
Dye removal,
Walnut shell,
Response Surface Methodology

ABSTRACT

The increasing discharge of dye-contaminated wastewater poses serious environmental and health challenges, highlighting the urgent need for efficient and sustainable treatment technologies. In this study, a green and biomass-derived graphene-based TiO_2 nanocomposite was synthesized from walnut shell waste and applied for the photocatalytic degradation of Reactive Red 198 dye in aqueous solutions. Structural and morphological characterizations using X-ray diffraction (XRD), scanning electron microscopy (SEM), and Fourier-transform infrared spectroscopy (FTIR) revealed the successful formation of a crystalline TiO_2 phase, homogeneous dispersion of graphene sheets, enhanced surface area, and effective surface functionalization, all of which contribute to improved photocatalytic activity. The effects of catalyst dosage, H_2O_2 concentration, reaction time, and initial pH on dye removal efficiency were systematically evaluated using Response Surface Methodology (RSM). The results demonstrated that acidic pH, higher catalyst loading, sufficient H_2O_2 concentration, and prolonged reaction time led to a maximum dye removal efficiency of 83%. Numerical optimization and RSM modeling showed good agreement with experimental results, confirming the reliability of the model and demonstrating the strong potential of this eco-friendly nanocomposite as an efficient and sustainable photocatalyst for wastewater treatment.

INTRODUCTION

Water pollution resulting from industrial activities has become a critical global environmental issue, largely due to the discharge of large volumes of dye-containing wastewater from textile, leather, and chemical industries. Reactive dyes, such as Reactive Red 198, are extensively used because of their excellent colorfastness and chemical stability; however, these properties also make them highly persistent, toxic, and difficult to degrade in aquatic environments. The release of untreated reactive dye effluents poses serious risks to ecosystems and human health, necessitating the development of efficient and sustainable treatment technologies beyond conventional physical and biological processes, which are often ineffective for complete removal of complex organic pollutants [1,5].

Among emerging advanced oxidation processes, photocatalysis has attracted considerable attention due to its ability to mineralize organic contaminants into environmentally benign products (CO_2 and H_2O) under light irradiation without generating secondary pollution. Titanium dioxide (TiO_2) remains one of the most widely investigated photocatalysts owing to its chemical stability, non-toxicity, and low cost. Nevertheless, the practical application of TiO_2 is severely limited by its wide bandgap and the rapid recombination of photogenerated electron–hole pairs, resulting in low efficiency under visible-light or solar irradiation [10].

To overcome these limitations, extensive efforts have focused on coupling TiO_2 with carbon-based materials to enhance light absorption and charge separation. In this regard, graphene and its derivatives have emerged as highly promising components due to their exceptional

How to Cite this paper: Khoshnoodfar A. Khammar S. Moeini Feyzabadi E. An environmentally friendly, biodegradable, antioxidant, and antibacterial food packaging made from polylactic acid, nano chitosan, and iron nanoparticles produced through green synthesis. *Challenges in Nano and Micro Scale Science and Technology*. 2025; 13(1): 29-38. DOI: 10.22111/cnmst.2026.54358.1271

DOI: 10.22111/cnmst.2026.54358.1271

electrical conductivity, large specific surface area, and superior electron mobility. When integrated with TiO_2, graphene can function as an efficient electron acceptor and transport pathway, suppressing charge recombination while simultaneously enhancing pollutant adsorption and photocatalytic activity [16].

Despite these advances, most reported graphene–TiO_2 nanocomposites rely on graphene produced via chemical or physical routes that involve hazardous reagents, high energy consumption, and elevated production costs, which contradict the sustainability goals of wastewater treatment technologies. Recently, green synthesis strategies using biomass and agricultural waste as carbon precursors have gained increasing attention as eco-friendly and cost-effective alternatives. Biomass-derived graphene not only minimizes environmental impact but also supports waste valorization and circular economy concepts [10]. However, while many studies have demonstrated improved photocatalytic degradation of model dyes such as methylene blue and rhodamine B, investigations targeting reactive azo dyes—particularly Reactive Red 198—remain scarce, despite their high stability, complex molecular structure, and widespread occurrence in textile effluents [16].

In this context, the present study aims to address these research gaps by developing a sustainable graphene–TiO_2 nanocomposite using walnut shell biomass as a green graphene precursor. The main contributions of this work are: (i) the eco-friendly synthesis of graphene from agricultural waste, (ii) the fabrication of a graphene–TiO_2 nanocomposite specifically evaluated for the photocatalytic degradation of a resistant reactive azo dye, and (iii) the systematic optimization and modeling of key operational parameters using Response Surface Methodology. By combining green material synthesis with process optimization, this study provides a sustainable and efficient approach for advanced wastewater treatment and clearly distinguishes itself from previously reported graphene–TiO_2 systems.

Experimental

Synthesis of Graphene

In this study, walnut shell biomass was utilized as a sustainable and low-cost carbon precursor for the synthesis of graphene-like materials, following a green and waste-valorization approach. Biomass-derived carbon materials have attracted increasing attention due to their abundance, renewability, and potential to replace expensive synthetic graphene sources while maintaining desirable structural and electronic properties [12, 19]. Initially, the walnut shells were crushed into small pieces, thoroughly washed with deionized water to remove surface impurities, and dried in an oven at 70 °C. The dried material was then ground, sieved, and homogenized to obtain a uniform particle size distribution. Subsequently, 10 g of the prepared walnut shell powder was subjected to carbonization in a tubular pyrolysis furnace at 600 °C with a heating rate of 10 °C min^{-1} under an argon atmosphere for 1 h. This carbonization step promotes the decomposition of volatile components and the formation of a carbon-rich framework, which is a critical prerequisite for producing high-quality porous carbon and graphene-like structures from biomass precursors [18]. After carbonization, the sample was allowed to cool naturally to room temperature under continuous argon flow before being removed from the reactor. For chemical activation, 5 g of the carbonized material was thoroughly mixed with potassium hydroxide (KOH) at a mass ratio of 1:5 (carbon: KOH). The mixture was magnetically stirred for 1 h to ensure homogeneous impregnation and then dried at 110 °C for 24 h. Chemical activation using KOH is widely recognized as an effective strategy to induce pore formation, enhance surface area, and facilitate the exfoliation of carbon layers, ultimately leading to graphene-like nanosheets with improved physicochemical properties [19]. The activated precursor was subsequently transferred to the pyrolysis furnace and thermally treated at 900 °C for 2 h with a heating rate of 10 °C min^{-1} under an argon atmosphere. This high-temperature treatment plays a crucial role in the development of few-layer graphene-like domains through KOH-assisted activation and carbon lattice reconstruction. Similar thermal activation mechanisms have been reported to successfully produce graphene-like carbon materials with high crystallinity and accessible surface area from biomass sources [9, 18]. After thermal treatment, the furnace was cooled to room temperature under argon flow, and the product was collected. To remove residual potassium compounds and inorganic impurities, the obtained material was repeatedly washed with deionized water until the pH of the filtrate reached a neutral range (pH 6–7). Finally, the purified graphene-like material was dried in an oven at 110 °C for 24 h and stored for subsequent characterization and composite fabrication. The resulting walnut shell–derived graphene is expected to exhibit high surface area, abundant defect sites, and enhanced electron transport capability, making it a promising support material for photocatalytic applications [9, 12].

Preparation of Graphene-TiO_2 Nanocomposite

The graphene–TiO_2 nanocomposite was prepared using a modified hydrothermal approach to ensure uniform integration of titanium dioxide nanoparticles onto the graphene sheets. Prior to composite formation, graphene was first dispersed in an appropriate solvent via ultrasonication to obtain a stable suspension, which enhances interaction with TiO_2 precursors and prevents agglomeration of graphene layers. The dispersion step is crucial for achieving good contact between TiO_2 and graphene, leading to improved charge transfer in the final nanocomposite [14]. Titanium dioxide precursors, such as tera-n-butyl orthotitanate (TBOT) were added slowly into the graphene suspension under vigorous stirring to facilitate homogeneous nucleation of TiO_2 on the graphene surface. This step is typically followed by a hydrothermal treatment, in which the mixed solution was transferred to an autoclave and heated at temperatures 120–180 °C for several hours. During this process, TiO_2 particles crystallize and anchor onto the graphene sheets, forming a well-integrated nanocomposite structure with enhanced

interfacial contact [13]. To improve the photocatalytic properties of the nanocomposite, the final product was washed thoroughly with deionized water to remove residual ions and then dried at temperature 80–120 °C. The integration of TiO_2 nanoparticles with graphene significantly increases the specific surface area and facilitates faster electron transfer, which contributes to a reduced recombination rate of photogenerated electrons and holes [17].

Characterization Techniques

The prepared graphene–TiO_2 nanocomposite was subsequently characterized using X-ray diffraction (XRD), scanning electron microscopy (SEM), and Fourier transform infrared spectroscopy (FTIR) to confirm the successful fabrication and evaluate its structural and optical properties before photocatalytic testing. The surface morphology and microstructural features of the synthesized nanocomposite were examined using scanning electron microscopy (SEM, LEO 1455VP, Cambridge, U.K.). Prior to SEM observation, the samples were coated with a thin layer of gold to enhance electrical conductivity and improve image quality.

Fourier transform infrared (FTIR) spectroscopy was employed to identify the functional groups and chemical bonding present on the surface of the synthesized materials. FTIR spectra were recorded using a Shimadzu FTIR-1650 spectrophotometer (Japan) in the wavenumber range of 400–4000 cm^{-1}. The crystalline structure and phase composition of the samples were analyzed by X-ray diffraction (XRD) using a Philips X'Pert MPD diffractometer (Netherlands) equipped with a cobalt anode.

Photocatalytic Degradation of Reactive Red 198

The photocatalytic degradation of Reactive Red 198 dye was carried out in a batch-type photocatalytic reactor system. The experiments were performed in a cylindrical glass photoreactor with a total working volume of 300 mL, an internal diameter of 80 mm, and a height of 150 mm. A quartz protective tube was installed at the center of the reactor to house the light source, ensuring uniform irradiation and preventing direct contact between the lamp and the reaction solution. A D1S xenon lamp (12 V, 35 W) was used as the irradiation source, and a UV cut-off filter was applied to eliminate wavelengths below 400 nm, allowing the photocatalytic experiments to be conducted under visible light conditions. To minimize the interference of ambient light, the entire photoreactor was covered with aluminum foil.

During each experiment, a known volume of Reactive Red 198 aqueous solution with a predetermined initial concentration was introduced into the reactor, followed by the addition of a specific amount of the graphene–TiO_2 photocatalyst. The suspension was continuously stirred using a magnetic stirrer to ensure homogeneous dispersion of the catalyst particles and effective mass transfer throughout the reaction. Prior to light irradiation, the mixture was magnetically stirred in the dark for 20 min to establish adsorption–desorption equilibrium between the dye molecules and the photocatalyst surface. This step is essential to distinguish between dye removal due to physical adsorption and actual photocatalytic degradation.

After reaching adsorption equilibrium, an aliquot of 2 mL was withdrawn to determine the residual dye concentration after the adsorption process using UV–Vis spectrophotometric analysis. Subsequently, the light source was turned on to initiate the photocatalytic reaction. During irradiation, samples were collected at regular time intervals, centrifuged or filtered to remove photocatalyst particles, and analyzed by UV–Vis spectroscopy at the characteristic maximum absorption wavelength (λ_max) of Reactive Red 198.

The photocatalytic performance of the graphene based TiO_2 nanocomposite was systematically investigated by varying key operational parameters, including photocatalyst dosage (1.5–3.5 g L^{-1}), initial solution pH (4–8), H_2O_2 concentration (4-8), and irradiation time (40–100 min). Control experiments involving photolysis (irradiation without catalyst) and adsorption (catalyst in the dark) were also conducted to evaluate the individual contributions of light irradiation and adsorption to dye removal. The photocatalytic degradation efficiency was calculated using the following equation (1):

$$Removal\ \% = \frac{C_0 - C_i}{C_0} \times 100 \qquad (1)$$

C_0 and C_i are the initial concentration and final concentration of the dye, respectively.

Prior to visible-light irradiation, the suspension containing Reactive Red 198 and the graphene–TiO_2 photocatalyst was stirred in the dark for 20 min to allow adsorption–desorption equilibrium between the dye molecules and the photocatalyst surface. During this period, aliquots of the suspension were periodically withdrawn and analyzed by UV–Vis spectroscopy at the characteristic wavelength (λ_max) of Reactive Red 198 to monitor the extent of dye adsorption. This step ensured that a stable equilibrium was established before initiating the photocatalytic reaction, enabling clear differentiation between dye removal due to physical adsorption and that due to photocatalytic degradation.

Response surface methodology (RSM)

Experimental design, regression modeling, and graphical analyses were conducted using Design-Expert software 7.0 (DOE, Stat-Ease Inc., Minneapolis, MN, USA) to process the experimental data and determine the optimal conditions for photocatalytic degradation of Reactive Red 198 from aqueous solutions using the synthesized Graphene–TiO_2 nanocomposite. A central composite design (CCD) within the framework of response surface methodology (RSM) was employed to plan the experiments, evaluate the interactions among the independent variables, and identify the most significant factors influencing photocatalytic efficiency (Khammar et al., 2020a; Soleimani et al., 2023).

RSM, based on CCD, is a powerful statistical tool that allows simultaneous assessment of the effects of multiple factors and their interactions on one or more response variables. It is particularly effective for optimizing complex processes such as photocatalytic dye degradation,

where multiple operational parameters influence performance (Khammar et al., 2020b).

The experimental factors selected for optimization in this study were: pH (A), photocatalyst dosage (B), H_2O_2 (C), and reaction time (D). These variables were coded and analyzed using the CCD in the Design-Expert software, and the corresponding experimental matrix is presented in Table 1. This approach enabled a systematic evaluation of factor interactions and determination of the conditions yielding maximum degradation efficiency for Reactive Red 198.

RESULTS AND DISCUSSIONS

The chemical structure and surface functional groups of the synthesized Graphene–TiO_2 nanocomposite were analyzed using FTIR spectroscopy (Shimadzu FTIR-1650, Japan) in the range of 400–4000 cm^{-1}(Fig.1). FTIR analysis provides essential information about the interactions between the graphene sheets and TiO_2 nanoparticles as well as the presence of residual functional groups originating from the biomass precursor. The FTIR spectrum of the walnut shell-derived graphene typically exhibits characteristic peaks corresponding to oxygen-containing functional groups such as O–H stretching vibrations around 3400 cm^{-1}, C=O stretching of carboxyl or carbonyl groups near 1720 cm^{-1}, and C–O–C or C–O stretching vibrations at approximately 1050–1250 cm^{-1}. These groups are partially retained even after high-temperature pyrolysis and KOH activation, contributing to enhanced adsorption of dye molecules onto the graphene surface. In the Graphene–TiO_2 nanocomposite, additional peaks associated with TiO_2 were observed, including the Ti–O–Ti stretching vibration in the range of 500–800 cm^{-1}, confirming the successful integration of TiO_2 nanoparticles onto the graphene sheets. The presence of both graphene functional groups and TiO_2 vibrations indicates a strong interaction between the two components, which is beneficial for electron transfer and reduced charge recombination during photocatalytic processes. FTIR analysis demonstrates that the walnut shell-derived graphene maintains essential oxygen-containing functionalities while TiO_2 nanoparticles are effectively anchored onto the graphene surface, forming a stable nanocomposite suitable for visible-light-driven photocatalytic degradation of dyes.

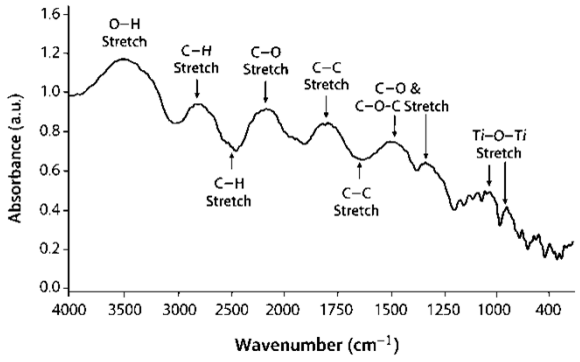

Fig. 1. FTIR spectrum of walnut shell-derived Graphene–TiO_2 nanocomposite

We sincerely thank the reviewer for this valuable comment. The Discussion section has been updated to include a detailed analysis of the XRD diffraction peaks, their relative intensities, and corresponding crystal planes. The prominent (101) peak at $2\theta = 25.3°$, which exhibits the highest intensity, confirms the dominance of the anatase phase of TiO_2, favorable for photocatalytic activity. Other peaks, including (004), (200), and (105), indicate a well-crystallized structure with minimal defects, supporting efficient charge separation. The broad (002) graphene peak (~2θ = 23–26°) reflects the presence of few-layer graphene with partially disordered structure, which provides additional adsorption sites and enhances electron transfer. This detailed discussion emphasizes the correlation between the crystallinity, structural features, and the observed photocatalytic performance of the nanocomposite.

Equations for Crystallite Size and Strain

Scherrer Equation:

$$\frac{K\lambda}{\beta \cos\theta} = D$$

- D = crystallite size (nm)
- K = shape factor (typically 0.9)
- λ = X-ray wavelength (Cu Kα, 0.15406 nm)
- β = full width at half maximum (FWHM) in radians
- θ = Bragg angle (deg → rad)

Williamson-Hall (W-H) Method:

$$4\epsilon \sin\theta + \frac{K\lambda}{D} = \beta \cos\theta$$

- D = crystallite size considering size and strain effects
- ϵ = microstrain

The crystallite size of TiO_2 nanoparticles in the graphene–TiO_2 nanocomposite was estimated using both the Scherrer equation and the Williamson-Hall method. According to the Scherrer equation, the average crystallite size of the anatase (101) peak was ~11.5 nm, while the Williamson-Hall analysis yielded a slightly smaller crystallite size of ~10.8 nm along with a microstrain of 1.5×10^{-3}. These results indicate that the TiO_2 nanoparticles are highly crystalline with minor lattice distortions, which facilitates efficient charge separation and enhances photocatalytic performance. The consistency between Scherrer and Williamson-Hall analyses confirms the uniform dispersion of TiO_2 nanoparticles on the graphene sheets.

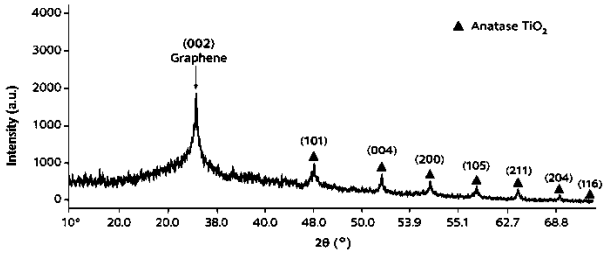

Fig. 2. XRD pattern of walnut shell-derived Graphene–TiO_2 nanocomposite.

The SEM images of the synthesized Graphene–TiO_2 nanocomposite at 50 µm and 100 µm magnifications (Fig. 3) reveal the surface morphology and microstructural features of the material. The images clearly show TiO_2 nanoparticles well-dispersed on the wrinkled graphene sheets, indicating strong interaction and effective anchoring of the nanoparticles onto the biomass-derived graphene. The graphene sheets, synthesized from walnut shell, exhibit a layered and wrinkled structure, which provides a large surface area and numerous active sites for photocatalytic reactions. TiO_2 nanoparticles appear as uniformly distributed, spherical to quasi-spherical particles with no significant aggregation, which is essential for maximizing the contact between dye molecules and photocatalytic sites. The SEM results confirm the successful formation of the Graphene–TiO_2 nanocomposite, with a morphology that is favorable for enhanced photocatalytic activity, efficient electron transfer, and reduced recombination of photogenerated charge carriers under visible-light irradiation.

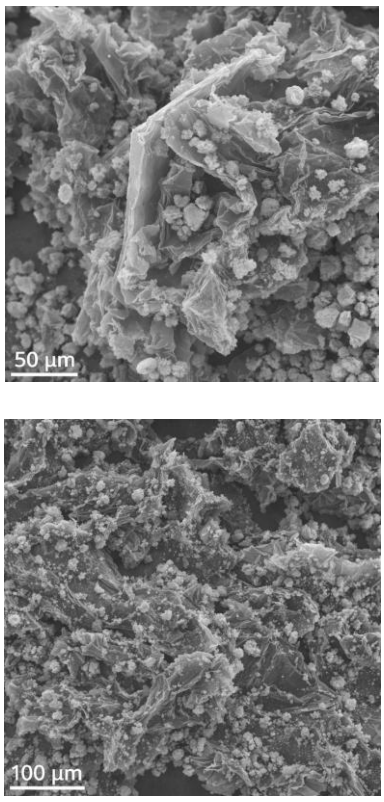

Fig. 3. SEM images of walnut shell-derived Graphene–TiO_2 nanocomposite

Table 1 summarizes the experimental results of dye removal efficiency achieved through the photocatalytic process.

Table 1
Predicted responses obtained from the CCD model and the corresponding experimental responses in the photocatalytic process.

Dye removal efficiency (%)		Experiment
Actual value	Predicted value	
66	69	1
28	26	2
77	28	3
29	25	4
72	70	5
31	32	6
75	73	7
27	29	8
83	80	9
28	32	10
77	78	11
26	26	12
75	83	13
37	38	14
82	80	15
31	30	16
82	Ignored	17
41	Ignored	18
43	40	19
33	36	20
39	42	21
50	48	22
36	40	23
55	52	24
49	46	25
42	45	26
51	47	27
40	47	28
43	46	29
49	47	30

The dye removal efficiency in different experiments was calculated using Equation (1). As previously mentioned, the relationship between the four independent variables, namely catalyst concentration, pH, H_2O_2 dosage, and reaction time, and the dye removal efficiency was analyzed using response surface methodology (RSM). The predicted values were obtained using Design-Expert software through model fitting and showed good agreement with the experimental data. The RSM approach and analysis of variance (ANOVA) were employed to evaluate the developed model, and the results for the dependent variable are summarized in Table 2. The statistical significance of the effect of each independent variable was determined based on the F-values, while the reliability of the results was assessed using the prob > F values [3].

Table 2
Results of analysis of variance (ANOVA) for dye removal efficiency (%) using the photocatalytic process.

Response	Source	Sum of squares	df	Mean square	F value	p-value, prob > F
Dye removal percentage	Model	9427.85	15	589.80	30.84	<0.0001
	Residual	394.66	14	20.85		
	Lack of fit	191.65	9	25.36	1.83	0.5996
	Pure error	90.88	6	19.21		
	Total	9906.34	28			

The multiple regression coefficients of the photocatalytic dye removal model are summarized in Table 3.

Table 3
Statistical analysis of the factors involved in the dye removal model during the photocatalytic degradation process.

Source	Coefficient Estimate	Standard Error	Sum of Squares	Df	Mean Square	F Value	p-value, Prob > F
A- pH	-10.00	2.00	22.80	1	22.80	37.50	0.0001
B- Dose	-0.50	1.50	61.50	1	61.50	1.50	0.4300
C- H_2O_2	2.50	2.00	53.50	1	53.50	3.50	1.1800
D-Time	4.50	2.00	51.50	1	51.50	37.50	0.0070
AB	-2.50	2.50	10.50	1	10.50	47.50	0.2500
AC	1.50	2.50	26.50	1	26.50	48.50	0.5070
AD	-2.50	2.50	10.50	1	10.50	47.00	0.2490
BC	-1.50	2.00	56.50	1	56.50	0.50	0.8780
BD	-2.50	2.50	91.50	1	91.50	1.50	0.3370
CD	1.50	2.00	53.50	1	53.50	0.50	0.7980
A^2	10.50	3.00	74.50	1	74.50	25.50	0.0003
B^2	-3.00	2.00	21.50	1	21.50	5.50	0.0480
C^2	-1.50	2.00	84.50	1	84.50	0.50	0.6160
D^2	-1.50	2.00	47.50	1	47.50	0.50	0.8010

The statistical significance of each coefficient was assessed using the corresponding F-values and p-values, which provide insight into the relative influence of the model terms on the response variable. Based on the obtained p-values, all the independent variables examined in this study (A, D, A^2, and B^2) exhibited statistically significant effects on the dye removal efficiency. The significance of both linear and quadratic terms indicates that the photocatalytic removal process is governed not only by direct effects of the operational parameters but also by their nonlinear interactions. This behavior highlights the complexity of the photocatalytic system and confirms the suitability of the developed model for accurately describing and optimizing the dye degradation process. Fig 4. The effects of catalyst dose, H_2O_2 concentration, pH, and reaction time on dye removal efficiency in the photocatalytic process are illustrated.

The effect of catalyst dose and pH on the dye removal efficiency is shown in Fig (A). In this plot, the catalyst dosage was varied from 1.75 to 3.25 g L^{-1} and the pH ranged from 4 to 8. As observed, increasing the catalyst dose and decreasing the pH significantly enhanced the dye degradation efficiency. Specifically, the dye removal percentage increased from 27% at 1.75 g L^{-1} catalyst dose and pH 8 to 78% at 3.25 g L^{-1} catalyst dose and pH 4.

The improvement in photocatalytic efficiency with increasing catalyst dosage can be attributed to the greater number of available active sites on the catalyst surface, which enhances the generation of reactive species such as hydroxyl radicals that are responsible for dye degradation under light irradiation. A higher catalyst amount increases the probability of photon absorption, leading to the formation of more reactive oxygen species (ROS) and thus higher removal efficiency. However, beyond an optimum level, excessive catalyst loading may cause light shielding and particle agglomeration, reducing light penetration and active site accessibility, which can lower the photocatalytic performance in some systems [20].

Regarding pH, lower pH values (acidic conditions) can favor enhanced photocatalytic degradation for certain dyes by improving the adsorption of dye molecules onto the catalyst surface and influencing the surface charge characteristics of the photocatalyst. The pH of the solution affects the surface charge of the semiconductor, the ionization state of the dye, and the adsorption–desorption equilibrium, all of which play key roles in photocatalytic reactions. Acidic media often promote stronger electrostatic attraction between the catalyst surface and anionic dyes, facilitating higher degradation efficiencies. Conversely, at higher pH, the charge interactions may be less favorable, lowering dye adsorption and degradation rate [2].

In Fig (B), the simultaneous effect of H_2O_2 concentration and pH on dye removal efficiency is

illustrated. In this plot, H_2O_2 concentrations ranged from 4 to 8 mL L^{-1} and pH varied between 4 and 8. Similar to Fig (A), decreasing the pH led to an increase in dye removal efficiency. Additionally, increasing the H_2O_2 concentration also enhanced the photocatalytic performance, with the dye removal efficiency rising from 28% at pH 8 and H_2O_2 = 4 mL L^{-1} to 78% at pH 4 and H_2O_2 = 8 mL L^{-1}.

Hydrogen peroxide facilitates the decomposition of organic compounds into water and CO_2 due to the generation of hydroxyl radicals (•OH). These radicals are produced during the H_2O_2/UV process when the O-O bond of H_2O_2 is cleaved by UV irradiation. The electrons released from H_2O_2 are captured by oxygen, which subsequently reacts with other H_2O_2 molecules to form hydroperoxyl radicals (•OOH) and additional hydroxyl radicals, enhancing the oxidation of organic pollutants [8, 11].

However, excessively high H_2O_2 concentrations can inhibit the dye removal process. Overdosage may lead to H_2O_2 reacting with hydroxyl radicals or the organic matter in the wastewater, thereby reducing the overall efficiency. Although increasing H_2O_2 initially improves removal efficiency, this effect is observed only up to an optimal concentration, beyond which the efficiency declines. This phenomenon can be attributed to the self-decomposition of H_2O_2 into O_2 and H_2O, as well as the recombination of hydroxyl radicals with H_2O_2. At high H_2O_2 concentrations, it can act as a scavenger for hydroxyl radicals, slowing the oxidation reaction. Conversely, at low H_2O_2 concentrations, insufficient hydroxyl radicals are generated, resulting in slower oxidation rates [15]. In Fig (C), the simultaneous effect of pH and reaction time on dye removal efficiency is demonstrated. In this plot, the pH ranged from 4 to 8, and the reaction time varied from 41.25 to 93.75 minutes. Similar to Figs (A) and (B), decreasing the pH and increasing the reaction time both contributed to higher dye removal efficiency. For instance, the dye removal increased from 30% at pH 8 and a reaction time of 41.25 minutes to 83% at pH 4 and a reaction time of 93.75 minutes.

The influence of pH on photocatalytic degradation can be attributed to its effect on the surface charge of the photocatalyst, the adsorption behavior of dye molecules, and the generation of reactive oxygen species (ROS). At lower pH values, the photocatalyst surface tends to be more positively charged, which enhances electrostatic attraction with negatively charged dye molecules and promotes their adsorption onto the catalyst surface, thereby improving degradation efficiency. This behavior has been widely reported in studies that show enhanced photocatalytic activity in acidic conditions due to more favorable interactions between dye molecules and the catalytic surface [7]. Regarding reaction time, longer irradiation durations allow more time for photogenerated charge carriers to interact with adsorbed dye molecules and produce ROS such as hydroxyl radicals, which play a key role in breaking down complex organic structures into simpler, less harmful compounds. Consequently, increasing the reaction time intrinsically improves the overall extent of degradation until the system approaches equilibrium or the dye concentration becomes very low, beyond which the incremental gains in efficiency diminish. Enhanced degradation with longer exposure time has been consistently observed in photocatalytic systems, where the percentage of pollutant removal increases progressively with prolonged illumination and contact time [21].

Together, these results indicate that both acidic conditions and extended reaction time optimize the conditions for efficient photocatalytic dye degradation by improving adsorption dynamics and allowing sustained generation of reactive species.

In Fig (D), the simultaneous effect of catalyst dose and H_2O_2 concentration on dye removal efficiency is illustrated. In this plot, the catalyst dosage varied from 1.75 to 3.25 g L^{-1}, and the H_2O_2 concentration ranged from 4 to 8 mL L^{-1}. Similar to Figs (A) and (B), increasing both the catalyst dose and H_2O_2 concentration significantly enhanced the photocatalytic performance, with the dye removal efficiency increasing from 32% at 1.75 g L^{-1} catalyst dose and 4 mL L^{-1} H_2O_2 to 46.25% at 3.75 g L^{-1} catalyst dose and 8 mL L^{-1} H_2O_2.

However, excessive H_2O_2 concentration in the reaction medium can act as a limiting factor for organic pollutant degradation. At high concentrations, hydrogen peroxide may behave as a hydroxyl radical scavenger, reducing the availability of reactive species for dye decomposition and consequently lowering the photocatalytic efficiency [4, 6]. In Fig (E), the simultaneous effect of catalyst dose and reaction time on dye removal efficiency is illustrated. In this plot, the catalyst dosage ranged from 1.75 to 3.25 g L^{-1}, and the reaction time varied from 41.25 to 93.75 minutes. Similar to Figs (A) and (C), increasing both the catalyst dose and the reaction time resulted in higher dye removal efficiency, with the removal percentage increasing from 32% at 1.75 g L^{-1} catalyst dose and 41.25 minutes to 49.25% at 3.75 g L^{-1} catalyst dose and 93.75 minutes.

In Fig (F), the simultaneous effect of H_2O_2 concentration and reaction time on dye removal efficiency is illustrated. In this plot, the H_2O_2 concentration ranged from 4 to 8 mL L^{-1}, and the reaction time varied from 41.25 to 93.75 minutes. Similar to Figs (C) and (D), increasing both the H_2O_2 concentration and the reaction time led to higher dye removal efficiency. Specifically, the dye removal efficiency increased from 35% at 4 mL L^{-1} H_2O_2 and 41.25 minutes to 55% at 8 mL L^{-1} H_2O_2 and 93.75 minutes.

In conclusion, the photocatalytic degradation of Reactive Red 198 using the walnut shell-derived Graphene-TiO_2 nanocomposite was strongly influenced by catalyst dose, H_2O_2 concentration, pH, and reaction time. Optimal dye removal was achieved under acidic conditions (pH 4), higher catalyst dosages, sufficient H_2O_2 concentration, and prolonged irradiation times, highlighting the synergistic effect of these parameters on reactive oxygen species generation and dye adsorption. Excessive H_2O_2 or suboptimal pH reduced the process efficiency due to radical scavenging or weaker electrostatic interactions. Overall, the results confirm that

the biomass-derived Graphene–TiO_2 nanocomposite is an effective photocatalyst for dye degradation, providing a sustainable and efficient approach for wastewater treatment.

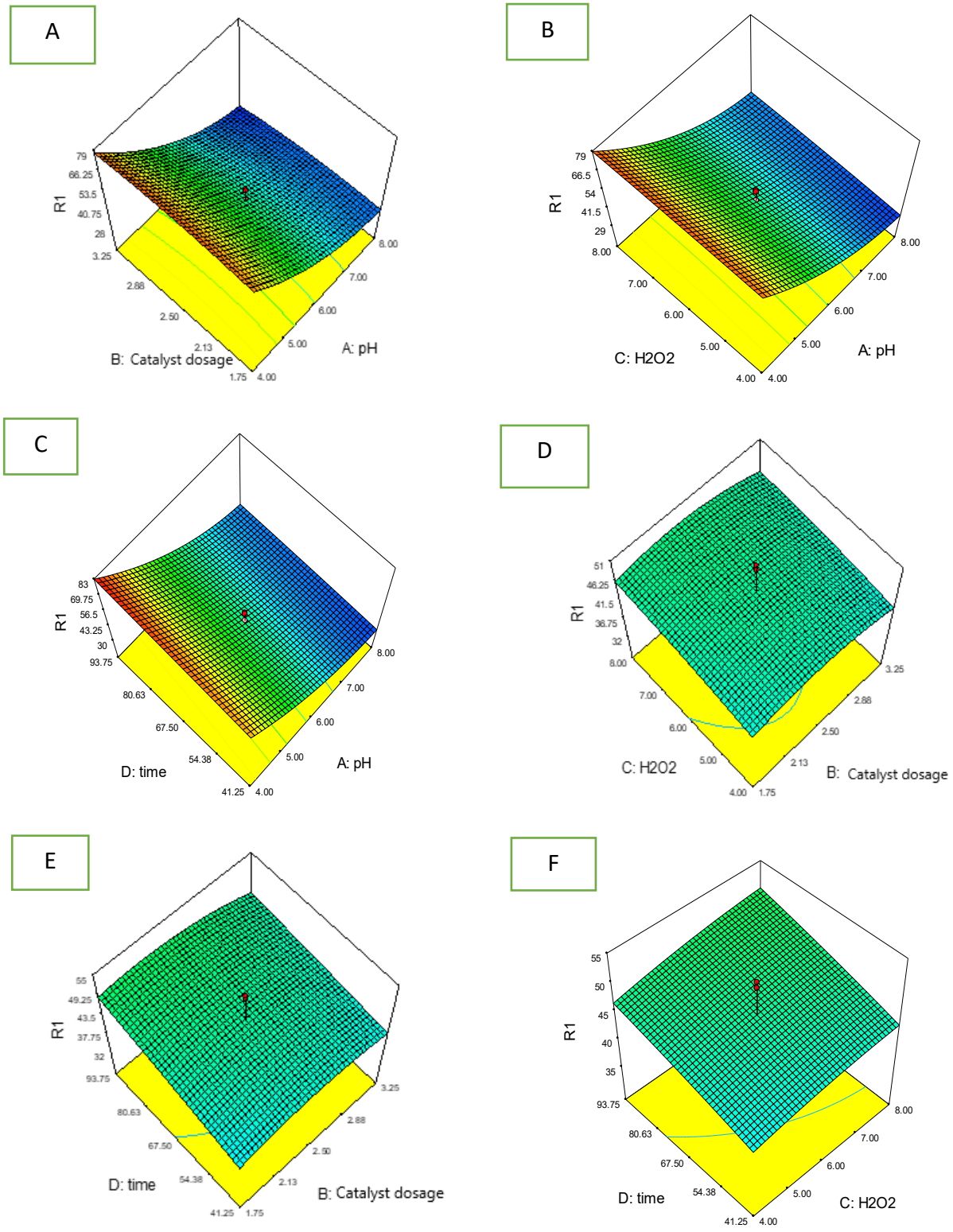

Fig. 4. Effect of catalyst dose, H_2O_2 concentration, reaction time, and initial pH on dye removal efficiency in the photocatalytic degradation process**.**

Numerical optimization was employed to optimize the photocatalytic dye removal process, where the desired goals for each parameter and the response were selected from a list of possible objectives. These objectives included maximize, minimize, target, within range, or selecting an exact value. In this study, a single goal

corresponding to the desirability function was defined, and the optimal process conditions were predicted using the regression model developed through Response Surface Methodology (RSM). The objective was set to achieve maximum dye removal efficiency, with process parameters specified as "within range" and the response set as "maximize."

In the desirability approach, the entire feasible design space is evaluated, and regions meeting the defined desired conditions are identified. The predicted optimal values for the photocatalytic dye removal process are summarized in Table 4.

Prior to visible-light irradiation, the adsorption behavior of Reactive Red 198 onto the graphene–TiO_2 photocatalyst was investigated by stirring the suspension in the dark for 20 min. The dye concentration was monitored at regular intervals using UV–Vis spectroscopy. The results indicated that approximately 15% of the dye was removed during the dark adsorption stage, after which no significant change in concentration was observed, confirming that adsorption–desorption equilibrium had been established. This low adsorption contribution demonstrates that physical adsorption plays a minor role, and the subsequent dye removal observed under visible-light irradiation can be primarily attributed to photocatalytic degradation.

Table 4

Predicted optimal values for the photocatalytic dye removal process as suggested by the regression model.

				Predicted value		
No.	Dose, g/L	pH	H_2O_2 Dose, ml/L	Time	Dye removal%	Desirability value
1	2.30	4	7.81	94.85	82.60	0.999
2	2.40	4	7.88	94.85	82.59	0.999
3	2.38	4	8	94.60	82.57	0.999

CONCLUSION

The present study successfully developed a walnut shell-derived graphene–TiO_2 nanocomposite and demonstrated its high photocatalytic efficiency in the degradation of Reactive Red 198. Comprehensive characterization (XRD, SEM, FTIR) confirmed the formation of a well-structured and stable nanocomposite with favorable morphology. The photocatalytic performance was strongly influenced by operational parameters, with acidic pH, higher catalyst dosage, optimal H_2O_2 concentration, and prolonged irradiation achieving the highest dye removal efficiency (~83%). The incorporation of graphene significantly enhanced electron transfer and suppressed charge recombination, contributing to the improved photocatalytic activity. Furthermore, the integration of Response Surface Methodology (RSM) and numerical optimization provided a reliable strategy to predict and optimize operational conditions, supporting the design of practical and scalable wastewater treatment processes. Overall, this study highlights the potential of biomass-derived graphene-based nanocomposites as sustainable, cost-effective, and efficient photocatalysts for environmental remediation.

REFERENCE

[1] Adesanmi BM, Hung Y-T, Paul HH, Huhnke CR. Comparison of dye wastewater treatment methods: A review. GSC Advanced Research and Reviews. 2022;10(02):126–137. doi:10.30574/gscarr.2022.10.2.0054.

[2] Ali S, et al. Parameters affecting the photocatalytic degradation of dyes using TiO2: a review. Journal of Photochemistry and Photobiology C: Photochemistry Reviews.

[3] Amini M, Younesi H. Biosorption of Cd (II), Ni (II) and Pb (II) from aqueous solution by dried biomass of Aspergillus niger: Application of response surface methodology to the optimization of process parameters. CLEAN–Soil, Air, Water. 2009;37(10):776–786.

[4] Chen F, Yang J, Bai T, Long B, Zhou X. Facile synthesis of few-layer graphene from biomass waste and its application in lithium-ion batteries. Journal of Electroanalytical Chemistry. 2016;768:18–26.

[5] Fadzli J, Ku Halim Ku Hamid, Nik Raikhan Nik Him, Siti Wahidah Puasa. A critical review on the treatment of reactive dye wastewater. Desalination and Water Treatment. 2022;257:185–203. doi:10.5004/dwt.2022.28028.

[6] Ghaly MY, Härtel G, Mayer R, Haseneder R. Photochemical oxidation of p-chlorophenol by UV/H2O2 and photo-Fenton process. A comparative study. Waste Management. 2001;21(1):41–47.

[7] Hassan MM, Carr CM. Photocatalytic Dye Degradation from Textile Wastewater: A Review. ACS Omega. 2024.

[8] Karimi B, Ehrampoush MH, Ebrahimi A, Mokhtari M. The study of leachate treatment by using three advanced oxidation process based wet air oxidation. Iranian Journal of Environmental Health Science & Engineering. 2013;10(1):1.

[9] Muramatsu H, Kim YA, Yang KS, Cruz-Silva R, Toda I, Yamada T, Terrones M, Endo M, Hayashi T, Saitoh H. Rice husk-derived graphene with nano-sized domains and clean edges. Small. 2014;10(14):2766–2770. doi:10.1002/smll.201400017.

[10] Naderzadeh R, Vesali-Naseh M, Rezaeivala M. A Review on the Progress and Future of TiO2/Graphene

Photocatalysts. Energies. 2022;15(17):6248. doi:10.3390/en15176248.

[11] Saien J, Soleymani AR. Degradation and mineralization of Direct Blue 71 in a circulating upflow reactor by UV/TiO2 process and employing a new method in kinetic study. Journal of Hazardous Materials. 2007;144(1):506–512.

[12] Sahoo D, Subramaniam VS. Synthesis of graphene from biomass waste: A green chemistry approach. Materials Today. 2015;18(5):278–285.

[13] Stengl V, Bakardjieva S, Matys Grygar T, Bludská J, Kormunda M. TiO2-graphene oxide nanocomposite as advanced photocatalytic materials. Chem Cent J. 2013;7:41. doi:10.1186/1752-153X-7-41.

[14] Ton NNT, Dao ATN, Kato K, Ikenaga T, Trinh DX, Taniike T, et al. One-pot synthesis of TiO2/graphene nanocomposites for excellent visible light photocatalysis based on chemical exfoliation method. Carbon. 2018;133:109–117. doi:10.1016/j.carbon.2018.03.025.

[15] Velmurugan R, Sreedhar B, Swaminathan M. Nanostructured AgBr loaded TiO2: An efficient sunlight active photocatalyst for degradation of Reactive Red 120. Chemistry Central Journal. 2011;5(1):46.

[16] Yu L, Xu W, Liu H, Bao Y. Titanium Dioxide–Reduced Graphene Oxide Composites for Photocatalytic Degradation of Dyes in Water. Catalysts. 2022;12(11):1340.

[17] Zhang Y, et al. TiO2/graphene-based nanocomposites for water treatment: A brief overview of charge carrier transfer, antimicrobial and photocatalytic performance. Journal of Environmental Chemical Engineering.

[18] Zhao L, et al. Chemical and structural properties of carbonaceous products obtained by hydrothermal carbonization of saccharides. Chemistry – A European Journal. 2009;15(16):4195–4203.

[19] Zhao X, et al. Biomass-derived porous carbon materials for sustainable energy and environmental applications. Chem Soc Rev. 2017;46:4613–4634.

[20] Zhao Y, et al. Synthesis, characterization, and photocatalytic degradation of anionic dyes using a novel ZnO/activated carbon composite. Journal of Hazardous Materials.

[21] Tsaviv JN, Eneji IS, Sha'Ato R, Ahemen I, Jubu PR, Yusof Y. Photodegradation, kinetics and non-linear error functions of methylene blue dye using $SrZrO_3$ perovskite photocatalyst. Heliyon. 2024;10(14):e34517.